SMALL-SIGNAL MODELING OF LCC RESONANT CONVERTER

Eric X. Yang, Fred C. Lee, and Milan M. Jovanovic

Virginia Power Electronics Center
Virginia Polytechnic Institute & State University
Blacksburg, VA 24061

Abstract *- The small-signal modeling technique based on the extended describing function concept is applied to LCC resonant converters. The analytical model developed includes both frequency control and phase-shift control. The small-signal equivalent circuit models are also derived and implemented in PSPICE. The models are in good agreement with the measurement data.*

I. INTRODUCTION

An LCC resonant converter (Fig. 1) shares the advantages of other resonant converters, including natural commutation desirable for BJT, GTO and SCR devices when the switching frequency is lower than the resonant frequency, and zero voltage switching suitable for MOSFETs when the switching frequency is higher than the resonant frequency. These characteristics make the LCC resonant converter a potential candidate for high power or high frequency application.

Besides the above features, the LCC resonant converter offers additional merits when compared with series resonant converters (SRCs) and parallel resonant converters (PRCs) [1, 2]. First, the series capacitor, C_s, makes the equivalent tank capacitance smaller; this results in an increase of the characteristic impedance of the resonant tank, and is helpful to limit the circulating current. Secondly, the voltage conversion characteristics allow the converter to operate in a wide load range (from full load to no load), where PRCs may lose regulation at full-load end and SRCs may lose regulation at light load end. This is because the LCC resonant converter behaves more like a PRC under light load, and an SRC under full load. Therefore, the circulating energy at light load is minimized. Thirdly, the LCC converter has an inherent short circuit protection.

Since the third order resonant tank increases the complexity of the circuit, it is difficult to apply the traditional sample-data modeling method [5, 7, 8] to LCC resonant converters. There has been no attempt in the literature addressing the small-signal modeling of the LCC resonant converter.

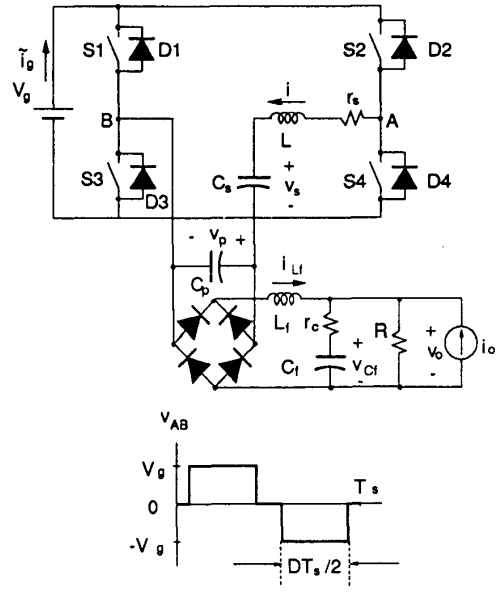

Fig. 1 Circuit diagram of an LCC resonant converter.

A recently developed small-signal modeling approach based on the extended describing function concept [9-11] is applied to the LCC resonant converter. The continuous-time model is derived in a closed form, and the equivalent circuit model is also obtained. The models include both frequency control and duty-cycle control (commonly referred to as phase-shift control). The conceptual diagram of the small-signal model is shown in Fig. 2.

In Fig. 2, $\hat{v}_g$ and $\hat{i}_o$ stand for small-signal perturbation of the line voltage and the output current, respectively; $\hat{f}_{SW}$ and $\hat{d}$ correspond to frequency control and duty-cycle control. The output variables include the perturbed average line current, $\hat{i}_g$, and the perturbed output voltage, $\hat{v}_o$. With the model, it is easy to obtain the commonly used small-signal transfer functions, such as control-to-output transfer function, line-to-output transfer function, input impedance, and output impedance.

†This work was supported by General Electric Corp., Schenectady, New York.

0-7803-0695-3/92 $3.00 © 1992 IEEE

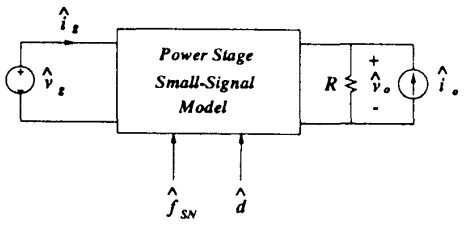

Fig. 2 **The conceptual diagram of the small-signal model of resonant converters. The control input could be switching frequency or duty-ratio.**

In Section II, an analytical small-signal model and an circuit model of LCC resonant converter are derived. Section III provides the experimental verification of these models. Section IV states the conclusions.

II. SMALL-SIGNAL MODELING OF LCC RESONANT CONVERTER

In this section, the systematic small-signal modeling procedure proposed in [10] is applied to LCC resonant converters. The step-by-step derivation of the small-signal models is illustrated.

A. Nonlinear State Equation

The circuit diagram of an LCC resonant converter is shown in Fig. 1. The active switch network generates a quasi-square wave voltage, v_{AB}, applied to the resonant tank. Under continuous tank current mode, the state equations of the power stage can be obtained, where the nonlinear terms are in bold face:

$$L\frac{di}{dt}+ir_s+v_s+v_p=v_{AB} \tag{1a}$$

$$C_s\frac{dv_s}{dt}=i \tag{1b}$$

$$C_p\frac{dv_p}{dt}+\boldsymbol{sgn(v_p)}i_{L_f}=i \tag{1c}$$

$$L_f\frac{di_{L_f}}{dt}+i_{L_f}r'_c+\left(1-\frac{r'_c}{R}\right)v_{C_f}=\boldsymbol{|\,v_p\,|}-r'_ci_o \tag{1d}$$

$$\frac{r_c}{r'_c}C_f\frac{dv_{C_f}}{dt}+\frac{1}{R}v_{C_f}=i_{L_f}+i_o. \tag{1e}$$

The output variables are the output voltage, v_o, and the averaged input current, i_g, of the power stage:

$$v_o=r'_ci_{L_f}+\left(1-\frac{r'_c}{R}\right)v_{C_f}+r'_ci_o, \tag{1f}$$

$$i_g=\frac{1}{T_s}\int_0^{T_s} i\frac{v_{AB}(t)}{v_g}dt, \tag{1g}$$

where

$$r'_C=r_C\,\|\,R. \tag{1h}$$

In this circuit, the output voltage is regulated either by modulating the switching frequency, ω_s, or by controlling the duty cycle, d, while maintaining a constant switching frequency. The operating point is determined by $\{v_g, i_o, R, \omega_s, d\}$.

B. Harmonic Approximation

The typical waveforms of the state variables are shown in Fig. 3. It is logical to make the assumption that the tank waveforms, $i(t)$, $v_s(t)$, and $v_p(t)$, be approximated by fundamental harmonics, and the output filter variables be approximated by the dc components. By making this assumption,

$$i\approx i_s(t)\sin\omega_s t+i_c(t)\cos\omega_s t \tag{2a}$$

$$v_s\approx v_{ss}(t)\sin\omega_s t+v_{sc}(t)\cos\omega_s t \tag{2b}$$

$$v_p\approx v_{ps}(t)\sin\omega_s t+v_{pc}(t)\cos\omega_s t. \tag{2c}$$

Notice that the envelope terms $\{i_s, i_c, v_{ss}, v_{sc}, v_{ps}, v_{pc}\}$ are slowly time varying, so the dynamic behavior of these terms can be investigated. The derivatives of $i(t)$, $v_s(t)$, and $v_p(t)$ are found to be:

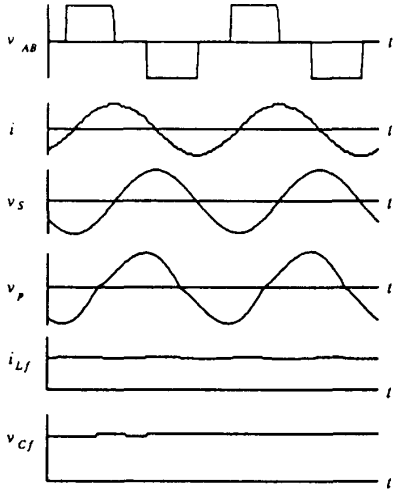

Fig. 3 **Typical waveforms of the state variables of an LCC resonant converter.**

$$\frac{di}{dt} \approx \left(\frac{di_s}{dt} - \omega_s i_c\right)\sin\omega_s t + \left(\frac{di_c}{dt} + \omega_s i_s\right)\cos\omega_s t \quad (3a)$$

$$\frac{dv_s}{dt} \approx \left(\frac{dv_{ss}}{dt} - \omega_s v_{sc}\right)\sin\omega_s t + \left(\frac{dv_{sc}}{dt} + \omega_s v_{ss}\right)\cos\omega_s t \quad (3b)$$

$$\frac{dv_p}{dt} \approx \left(\frac{dv_{ps}}{dt} - \omega_s v_{pc}\right)\sin\omega_s t + \left(\frac{dv_{pc}}{dt} + \omega_s v_{ps}\right)\cos\omega_s t \quad (3c)$$

C. Extended Describing Function

By employing the extended describing function concept [10], the nonlinear terms in Eq. (1) can be approximated either by the fundamental harmonic terms or by the dc terms, to give:

$$v_{AB}(t) \approx f_1(d, v_g)\sin\omega_s t \quad (4a)$$

$$sgn(v_p) i_{L_f} \approx f_2(v_{ps}, v_{pc}, i_{L_f})\sin\omega_s t + f_3(v_{ps}, v_{pc}, i_{L_f})\cos\omega_s t \quad (4b)$$

$$|v_p| \approx f_4(v_{ps}, v_{pc}) \quad (4c)$$

$$i_g \approx f_5(d, i_s). \quad (4d)$$

These $\{f_i(\cdot\,\cdot)\}$ are called extended describing functions (EDFs). They are functions of the operating conditions and the harmonic coefficients of the state variables. The EDF terms can be calculated by making Fourier expansions of the nonlinear terms, to yield:

$$f_1(d, v_g) = \frac{4}{\pi}\sin\left(\frac{\pi}{2}d\right)v_g \quad (4e)$$

$$f_2(v_{ps}, v_{pc}, i_{L_f}) = \frac{4}{\pi}\frac{v_{ps}}{A_p} i_{L_f} \quad (4f)$$

$$f_3(v_{ps}, v_{pc}, i_{L_f}) = \frac{4}{\pi}\frac{v_{pc}}{A_p} i_{L_f} \quad (4g)$$

$$f_4(v_{ps}, v_{pc}) = \frac{2}{\pi}A_p \quad (4h)$$

$$f_5(d, i_s) = \frac{2}{\pi}\sin\left(\frac{\pi}{2}d\right)i_s, \quad (4i)$$

where

$$A_p = \sqrt{v_{ps}^2 + v_{pc}^2}$$

is the peak voltage of the parallel resonant capacitor.

D. Harmonic Balance

With the small-signal modulation frequency lower than the switching frequency [10], by substituting Eqs. (2-4) into Eq. (1), and by equating the coefficients of dc, sine, and cosine terms respectively, we obtain:

$$L\left(\frac{di_s}{dt} - \omega_s i_c\right) + r_s i_s + v_{ss} + v_{ps} = \frac{4}{\pi}V_g \sin\left(\frac{\pi}{2}d\right) \quad (5a)$$

$$L\left(\frac{di_c}{dt} + \omega_s i_s\right) + r_s i_c + v_{sc} + v_{pc} = 0 \quad (5b)$$

$$C_s\left(\frac{dv_{ss}}{dt} - \omega_s v_{sc}\right) = i_s \quad (5c)$$

$$C_s\left(\frac{dv_{sc}}{dt} + \omega_s v_{ss}\right) = i_c \quad (5d)$$

$$C_p\left(\frac{dv_{ps}}{dt} - \omega_s v_{pc}\right) + \frac{4}{\pi A_p}i_{L_f} v_{ps} = i_s \quad (5e)$$

$$C_p\left(\frac{dv_{pc}}{dt} + \omega_s v_{ps}\right) + \frac{4}{\pi A_p}i_{L_f} v_{pc} = i_c \quad (5f)$$

$$L_f\frac{di_{L_f}}{dt} + i_{L_f} r'_c + \left(1 - \frac{r'_c}{R}\right)v_{c_f} = \frac{2}{\pi}A_p - r'_c i_o \quad (5g)$$

$$\frac{r_c}{r'_c}C_f\frac{dvc_f}{dt} + \frac{1}{R}v_{C_f} = i_{L_f} + i_o \quad (5h)$$

Equation (5) is a modulation equation. It is a nonlinear large-signal model of the LCC resonant converter power stage. It is important that the inputs of Eq. (5), $\{v_g, \omega_s, d, i_o\}$, are slow varying with respect to the switching frequency, so the modulation equation can be readily perturbed and linearized at certain operating points.

The corresponding output equations are:

$$v_o = r'_c(i_{L_f} + i_o) + \left(1 - \frac{r'_c}{R}\right)v_{C_f} \quad (5i)$$

$$i_g = \frac{2}{\pi}i_s \sin\left(\frac{\pi}{2}d\right). \quad (5j)$$

E. Steady-State Solution:

Under steady-state conditions, the new state variables of the modulation equation do not change with time. Upper case letters are used below to denote the steady-state values. For a given operating point $\{V_g, D, \Omega_s, I_o, R\}$, if we let the derivatives in Eq. (5) be zeros, and set the dc bias of the external current source I_o to zero, then the steady-state solution can be obtained by solving Eq. (5) (Appendix A).

The steady-state solution provides the results of the dc analysis of LCC resonant converters. For example, when the circuit has no loss, the voltage conversion ratio is given by:

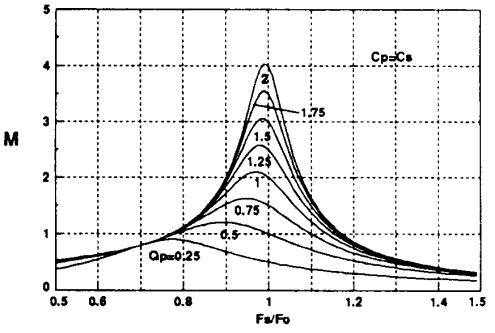

Fig. 4 **Voltage conversion ratio of an LCC resonant converter based on the steady-state solution of modulation equation.**

$$M(\Omega_s, D, R) = \frac{V_o}{V_g} = \frac{V_{Cf}}{V_g}$$

$$= \frac{\Omega_s C_s R \sin(D\pi/2)}{\sqrt{(1-\Omega_s^2 L C_s)^2 + (R_e \Omega_s (C_p + C_s)(1-\Omega_s L C_e))^2}} \quad .(6)$$

A result similar to Eq. (6) can be found in [2]. The voltage conversion ratio is the function of the switching frequency, the duty ratio, and the load. It is shown in Fig. 4 for the duty ratio equal to one ($D = 1$), where

$$Q_p = \frac{R}{Z_o} \quad Z_o = \sqrt{\frac{L}{C_e}} \quad F_o = \frac{1}{2\pi\sqrt{LC_e}} \quad C_e = \frac{C_s C_p}{C_s + C_p}$$

F. Perturbation and Linearization

By perturbing the large-signal model (Eq. (5)) around the operating point,

$$v_g = V_g + \hat{v}_g \qquad d = D + \hat{d}$$
$$i_o = 0 + \hat{i}_o \qquad \omega_s = \Omega_s + \hat{\omega}_s,$$

and by making linearization under the small-signal assumption, we obtain the following model:

$$L\frac{d\hat{i}_s}{dt} = -r_s\hat{i}_s + Z_L\hat{i}_c - \hat{v}_{ss} - \hat{v}_{ps} + k_v\hat{v}_g + E_d\hat{d} + E_s\hat{f}_{SN} \quad (7a)$$

$$L\frac{d\hat{i}_c}{dt} = -r_s\hat{i}_c - Z_L\hat{i}_s - \hat{v}_{sc} - \hat{v}_{pc} + E_c\hat{f}_{SN} \quad (7b)$$

$$C_s\frac{d\hat{v}_{ss}}{dt} = \hat{i}_s + G_s\hat{v}_{sc} + J_{ss}\hat{f}_{SN} \quad (7c)$$

$$C_s\frac{d\hat{v}_{sc}}{dt} = \hat{i}_c - G_s\hat{v}_{ss} - J_{sc}\hat{f}_{SN} \quad (7d)$$

$$C_p\frac{d\hat{v}_{ps}}{dt} = \hat{i}_s - g_{ps}\hat{v}_{ps} + g_{sc}\hat{v}_{pc} - 2k_s\hat{i}_{L_f} + J_{ps}\hat{f}_{SN} \quad (7e)$$

$$C_p\frac{d\hat{v}_{pc}}{dt} = \hat{i}_c + g_{cs}\hat{v}_{ps} - g_{pc}\hat{v}_{pc} - 2k_c\hat{i}_{L_f} + J_{pc}\hat{f}_{SN} \quad (7f)$$

$$L_f\frac{d\hat{i}_{L_f}}{dt} = k_s\hat{v}_{ps} + k_c\hat{v}_{pc} - r'_c\hat{i}_{L_f} - \frac{R}{R+r_c}\hat{v}_{Cf} - r'_c\hat{i}_o \quad (7g)$$

$$C_f\frac{d\hat{v}_{Cf}}{dt} = \frac{r'_c}{r_c}\left(\hat{i}_{L_f} - \frac{\hat{v}_{Cf}}{R} + \hat{i}_o\right) \quad (7h)$$

where the input variables are $\{\hat{v}_g, \hat{d}, \hat{f}_{SN}, \hat{i}_o\}$, standing for perturbed line voltage, duty-ratio, normalized switching frequency, and load current, respectively. The output part of the small-signal model is given by:

$$\hat{v}_o = r'_c(\hat{i}_{L_f} + \hat{i}_o) + \frac{R}{R+r_c}\hat{v}_{Cf} \quad (7i)$$

$$\hat{i}_g = \frac{2}{\pi}\sin\left(\frac{\pi}{2}D\right)\hat{i}_s + J_d\hat{d} \quad . \quad (7j)$$

This is a unified power-stage model with standard form as shown in Fig. 2. The model is time-continuous with parameters defined in Appendix B.

G. Equivalent Circuit Model

Since the small-signal model can be expressed by a linear state equation, the equivalent circuit model can be found from Eq. (7) by using the network synthesis, as shown in Fig. 5.

The circuit model has two parts: resonant tank part and output filter part. The output filter part is the realization of Eqs. (7g, 7h). Comparing with the circuit in Fig. 1, it is easy to see the rectified tank voltage, $|v_p|$, is replaced by the controlled voltage sources $\{k_s v_{ps}, k_c v_{pc}\}$.

The resonant tank part has a loop

$$\{0 \to 1 \to 2 \to 3 \to 4 \to 5 \to 6 \to 0\}$$

which is the realization of Eq. (7a) according to Kirchoff's voltage law (KVL). Equations (7c) and (7e) corresponds to Kirchoff's current law (KCL) of the node 5 and node 6, respectively. Notice the following controlled sources are defined to simplify the drawing:

$$\hat{v}_{in} = k_v\hat{v}_g + E_d\hat{d} \quad (8a)$$

$$\hat{j}_{ss} = G_s\hat{v}_{sc} + J_{ss}\hat{f}_{SN} \quad (8b)$$

$$\hat{j}_{ps} = g_{sc}\hat{v}_{pc} - 2k_s\hat{i}_{L_f} + J_{ps}\hat{f}_{SN} \quad (8c)$$

It is similar to synthesize the other part of the resonant tank from Eqs. (7b), (7d), and (7f) according KVL and KCL, where

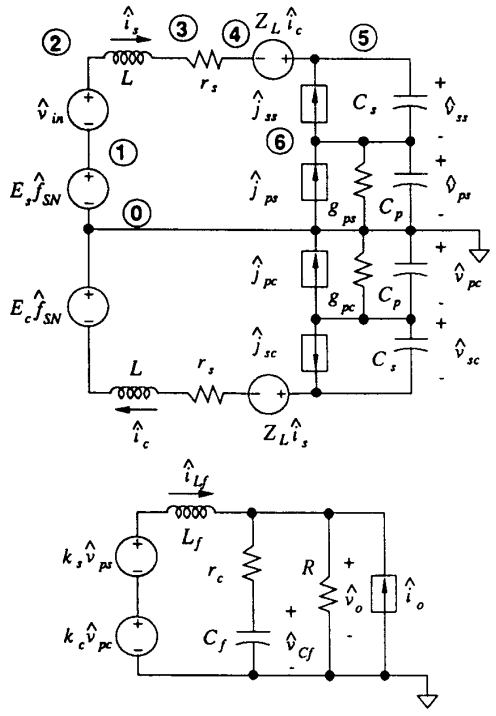

Fig. 5 **Small-signal equivalent circuit model of LCC resonant converters.**

$$\hat{j}_{sc} = G_s \hat{v}_{ss} + J_{sc} \hat{f}_{SN} \qquad (8d)$$

$$\hat{j}_{pc} = g_{cs} \hat{v}_{ps} - 2k_c \hat{i}_{L_f} + J_{pc} \hat{f}_{SN} \quad . \qquad (8e)$$

In the complete small-signal circuit, the resonant tank and output filter talk to each other by controlled sources. The resistor r_s represent the conduction loss of the resonant tank. The resistors paralleled to the capacitor C_p are not physically in the circuit, they are the small-signal resistances which will cause damping to output filter.

This circuit model can be easily implemented in PSPICE (Appendix C).

III. EXPERIMENTAL VERIFICATION

A high-frequency full-bridge LCC resonant converter was built and measured to verify the small-signal models derived in Section II. The circuit parameters were:

$$L = 36.3\mu H \qquad C_s = 1.23nF$$

$$C_p = 0.93nF \qquad L_f = 37.1\mu H$$

$$C_f = 1.19\mu F \qquad r_c = 0.973\Omega$$

$$F_o = 1.15MHz \qquad Z_o = 262\Omega.$$

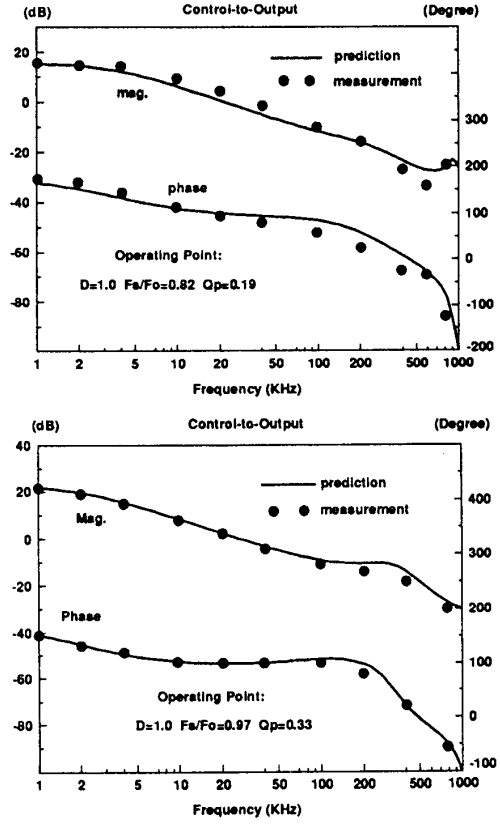

Fig. 6 **Frequency-to-Output Transfer Functions. The switching frequency is the control variable. The duty-ratio is not modulated.**

The frequency-control transfer functions are shown in Fig. 6, where the model predictions match the measurement data very well up to the switching frequency. This verification supports the conclusion in [10] that the harmonic balance of this modeling approach allows the modulation frequency to sweep up to one-half of the output ripple frequency. Figure 6 also shows that the small-signal models are valid for low Q (heavy load) operating condition, and the switching frequency can be very close to the resonant frequency.

The duty-ratio-control transfer functions are shown in Fig.7. These transfer functions have low-frequency dynamics and high-frequency dynamics [6]. The low-frequency dynamics are contributed by the output filter which is heavily damped by the output impedance of the resonant tank. The output filter poles are usually well separated. The high-frequency dynamics are the result of the interaction of the switching frequency and the resonant frequency; usually, a double-pole is observed

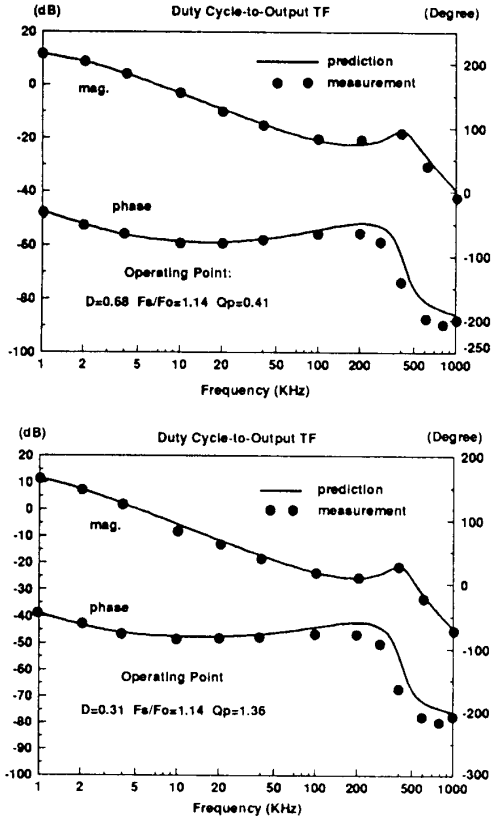

Fig. 7 **Duty-Ratio-to-Output Transfer Functions. The duty-ratio is the control variable. The switching frequency is not modulated.**

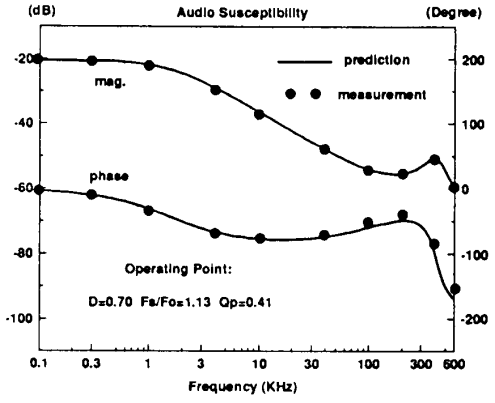

Fig. 8 **Audio Susceptibility.**

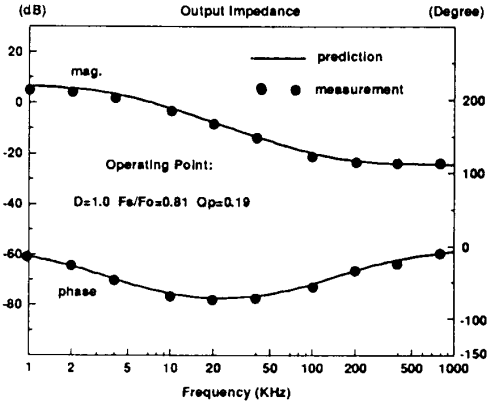

Fig. 9 **Output-Impedance.**

at the beat frequency, which is roughly the difference between of the switching frequency and the resonant frequency. The high-frequency dynamics are correctly predicted by the models. Results also show that the damping of the high frequency double-pole is determined by the loss of resonant tank, but not by the load resistance. It is important to point out that the location of the high-frequency double-pole is heavily affected by the operating point and the design of the power stage. This issue will be further addressed in another paper.

The line-to-output transfer function is shown in Fig. 8. Besides the good match between the model predictions and the measurement data, the dynamic pattern of audio susceptibility is quite similar to the control-to-output transfer functions.

The predicted and measured output impedance is shown in Fig. 9. The magnitude at the low-frequency end is determined by the load resistance and the output resistance of the resonant tank, while the magnitude at the high-frequency end is determined by the esr of the output capacitor.

IV. CONCLUSION

In this paper, the LCC resonant converter is modeled using the extended describing function technique. The continuous-time small-signal model is derived in an analytical form, which includes both frequency control and phase-shift control. The equivalent circuit model is also synthesized to facilitate the analysis using popular circuit analysis programs such as PSPICE. The models are accurate up to the switching frequency (half of the output ripple frequency) and not restricted to high Q operating conditions. The experimental results show that the model predictions agree well with the mea-

surement data. The high-frequency dynamics of LCC resonant converters around the beat-frequency can be accurately modeled. The models can be employed in the control loop design of LCC resonant converters.

REFERENCES

[1] A. K. S. Bhat, S. B. Dewan, "Analysis and design of a high-frequency resonant converter using LCC-type commutation," IEEE Trans. Power Electron., Vol. 2, no. 4, pp. 291-301, 1987.

[2] R. L. Steigerwald, "A comparison of half-bridge resonant converter topologies," IEEE Trans. Power Electron., Vol. 3, no. 2, pp. 174-182, 1988.

[3] I. Bataresh, R. Liu, C. Q. Lee, and A. K. Upadhyay, "150 Watts and 140 KHz multi-output LCC-type parallel resonant converter," Proc. APEC, pp. 221-230, 1989.

[4] C. Q. Lee, S. Sooksatra, and R. Liu, "Constant frequency controlled full-bridge LCC-type parallel resonant converter," Proc. IEEE APEC, pp. 587-593, 1991.

[5] V. Vorperian and S. Cuk, "Small-signal analysis of resonant converters," in IEEE Power Electronics Specialists' Conf. Rec., pp. 269-282, 1983.

[6] V. Vorperian, "Approximate small-signal analysis of the series and parallel resonant converters," IEEE Trans. Power Electronics, Vol. 4, no. 1, pp. 15-24, 1989.

[7] A. Witulski and R. Erickson, "Small-signal ac equivalent circuit modeling of the series resonant converter," in IEEE Power Electronics Specialists' Conf. Rec., pp. 693-704, 1987.

[8] M. G. Kim, J. H. Lee, J. H. Ko, and M. J. Youn, "A discrete time domain modeling and analysis of controlled parallel resonant converter," in IEEE Power Electronics Specialists' Conf. Rec., pp.730-736, 1991.

[9] S. Sanders, J. Noworolski, X. Liu, and G. Verghese, "Generalized averaging method for power conversion circuits," in IEEE Power Electronics Specialists' Conf. Rec., pp.273-290, 1989.

[10] E. X. Yang, F. C. Lee, and M. M. Jovanovic, "Small-signal modeling of power electronic circuits using extended describing function concept," in Proc. VPEC PES, pp. 167-178, 1991.

[11] E. X. Yang, F. C. Lee, and M. M. Jovanovic, "Extended describing function technique applied to the modeling of resonant converters," in Proc. VPEC PES, pp. 179-191, 1991.

APPENDIX A
STEADY STATE SOLUTION OF THE MODULATION EQUATION

$$I_s = V_e \Omega_s C_s \frac{(\beta - \alpha \Omega_s C_p R_e)}{\alpha^2 + \beta^2}$$

$$I_c = V_e \Omega_s C_s \frac{(\alpha + \beta \Omega_s C_p R_e)}{\alpha^2 + \beta^2}$$

$$V_{ss} = V_e \frac{(\alpha + \beta \Omega_s C_p R_e)}{\alpha^2 + \beta^2}$$

$$V_{sc} = V_e \frac{(-\beta + \alpha \Omega_s C_p R_e)}{\alpha^2 + \beta^2}$$

$$V_{ps} = V_e \frac{\beta \Omega_s C_s R_e}{\alpha^2 + \beta^2}$$

$$V_{pc} = V_e \frac{\alpha \Omega_s C_s R_e}{\alpha^2 + \beta^2}$$

$$A_p = V_e \frac{\Omega_s C_s R_e}{\sqrt{\alpha^2 + \beta^2}}$$

$$I_{L_f} = \frac{2 A_p}{\pi R}$$

$$V_{C_f} = \frac{2}{\pi} A_p$$

where

$$V_e = \frac{4}{\pi} V_g \sin\left(\frac{2}{\pi} d\right)$$

$$\alpha = 1 - \Omega_s^2 L C_s - R_e r_s \Omega_s^2 C_p C_s$$

$$\beta = R_e \Omega_s (C_p + C_s)\left(1 - \Omega_s^2 L C_e + \frac{r_s}{R_e} \frac{C_e}{C_p}\right)$$

$$R_e = \frac{\pi^2}{8} R, \quad C_e = \frac{C_s C_p}{C_s + C_p}$$

APPENDIX B
PARAMETERS OF THE SMALL-SIGNAL MODEL

$$k_v = \frac{4}{\pi} \sin\left(\frac{\pi}{2} D\right)$$

$$E_d = 2 V_g \cos\left(\frac{\pi}{2} D\right)$$

$$E_s = I_c \omega_o L$$

$$E_c = -I_s \omega_o L$$

$$Z_L = \Omega_s L$$

$$G_s = \Omega_s C_s$$

$$J_{ss} = V_{sc} \omega_o C_s$$

$$J_{sc} = V_{ss} \omega_o C_s$$

$$g_{ps} = \frac{1}{R_e}\frac{\alpha^2}{\alpha^2+\beta^2}$$

$$g_{pc} = \frac{1}{R_e}\frac{\beta^2}{\alpha^2+\beta^2}$$

$$g_{sc} = \Omega_s C_p + \frac{1}{R_e}\frac{\alpha\beta}{\alpha^2+\beta^2}$$

$$g_{cs} = -\Omega_s C_p + \frac{1}{R_e}\frac{\alpha\beta}{\alpha^2+\beta^2}$$

$$k_s = \frac{2}{\pi}\frac{V_{ps}}{A_p}$$

$$k_c = \frac{2}{\pi}\frac{V_{pc}}{A_p}$$

$$J_{ps} = V_{pc}\omega_o C_p$$

$$J_{pc} = -V_{ps}\omega_o C_p$$

$$J_d = I_s \cos\left(\frac{\pi}{2}D\right)$$

APPENDIX C
PSPICE CODES OF CIRCUIT MODEL

```
*Small-Signal Circuit Model of LCC
*The CKT parameters:
* L=36.3uH, Cs=1.23nF, Cp=0.93nF,
* Lf=37.1uH, Cf=1.19uF, rc=0.973 Ohm
*Operating point:
* D=1.0, Fs/Fo=0.97, Qp=0.33, Vg=81.7V
* The Injected Signals
Vg  20  0  ac  0
Rx1  20  0  1k
Vfsn  30  0  ac  1
Rx2  30  0  1k
Is  0  17  ac  0
* Sample Input Current --- v(40)
Flin  0  40  Vpis  0.637
Rlin  40  0  1

* The Upper Part of Resonant Tank (SINE)
Es  1  0  30  0  -78.9
EKv  2  1  20  0  1.27
VPis  2  3  dc  0
Ls  3  4  36.3uH
rss  4  5  78.5
HZLs  6  5  VPic  254
Css  6  7  1.23nF
Gs1  7  6  13  12  0.0086
GJss  7  6  30  0  -0.531
Cps  7  0  0.93nF
Rgps  7  0  130
Gsc  0  7  0  13  0.0029
F2ks  7  0  VPio  0.538
GJps  0  7  30  0  -0.317

* The Lower Part of Resonant Tank (COSINE)
Ec  0  8  30  0  -135
VPic  9  8  dc  0
Lc  10  9  36.3uH
rsc  11  10  78.5
HZLc  12  11  VPis  254
Csc  13  12  1.23nF
Gs2  13  12  6  7  0.0086
GJsc  13  12  30  0  -0.311
Cpc  0  13  0.93nF
Rgpc  0  13  596
Ggcs  13  0  7  0  -0.0101
F2kc  0  13  VPio  -1.15
GJpc  13  0  30  0  -0.148
* The Ouput Low Pass Filter
Ekc  14  0  0  13  -0.577
Eks  15  14  7  0  0.269
Vpio  15  16  DC  0
Lf  16  17  37.1uH
rc  17  18  0.973
Cf  18  0  1.19uF
R  17  0  87.4
.ac  dec  20  1KHz  1.0e6Hz
.print ac  vdb(17) vp(17)
.probe
.END
```